ELSEVIER

Journal of Nuclear Materials 241–243 (1997) 374–378

journal of nuclear materials

Kinetic simulation of parallel transport and ELM propagation in the Alcator C-Mod tokamak

O.V. Batishchev [a,b,c], A.A. Batishcheva [a], P.J. Catto [a,b], S.I. Krasheninnikov [a,d,*], B. LaBombard [a], B. Lipschultz [a], D.J. Sigmar [a]

[a] *Massachusetts Institute of Technology, Cambridge, MA 02139, USA*
[b] *Lodestar Research Corporation, Boulder, CO 80301, USA*
[c] *Keldysh Institute for Applied Mathematics, 125047 Moscow, Russia*
[d] *Kurchatov Institute of Atomic Energy, 123098 Moscow, Russia*

Abstract

The Fokker–Planck code ALLA [1] is employed to investigate parallel electron transport for plasma parameters and connection lengths typical of the Alcator C-Mod tokamak. A non-stationary 1D-2V purely kinetic model of scrape-off layer (SOL) plasmas is adopted which takes into account e–e and e–i Coulomb collisions, the self-consistent parallel electric field, and the sheath potential. We numerically study the effects of an enhanced (or depleted) suprathermal tail of the electron distribution on the Langmuir divertor and fast-scanning (FS) probe measurements, and edge localized mode (ELM) bursts.

Keywords: SOL plasmas; Kinetic analysis

1. Introduction

Alcator C-Mod operates with relatively cold and dense plasmas compared to other tokamaks. Typical mean plasma densities and temperatures of SOL plasmas are $n_p \approx 10^{14}$ cm^{-3} and $T_p \approx 30$ eV. The ratio γ of the Coulomb mean-free path $\lambda_c(cm) \approx 10^{12} T_p^2(eV)/n_p(cm^{-3})$ to half the connection length $L \approx 10^3$ cm is $1/100$ for open magnetic line averaged C-Mod plasma parameters. For this value the electron distribution is almost Maxwellian for thermal particles with energies $\varepsilon \leq T_p$, but departs from Maxwellian for suprathermal electrons with energies $\varepsilon > 2\text{–}3T_p$ because of the quadratic dependence of λ_c on energy ($\gamma(\varepsilon) \propto \varepsilon^2$).

The preceding indicates that the electron distribution function will have a Maxwellian bulk and non-Maxwellian tail due to the non-local behavior of Coulomb collisions in the presence of temperature gradients. A small change in the hot electron population can cause a significant change in the SOL plasma flow because these electrons determine the Spitzer–Harm heat conductivity [2] and the plasma–neutral interaction rates. Tail effects are especially important for detached SOL plasma flows [3] with low plasma temperatures ($T_d \approx 2$ eV) at the plate and strong temperature variations in the divertor region. Short mean free path expansions [4] used in fluid codes can fail in such a regime, making kinetic modeling necessary [5–10].

The suprathermal electrons also determine the electron temperature measured by divertor and reciprocating probes as discussed in Section 3. For example, the floating potential for a deuterium plasma is $\approx 3T_p$. The heating of the probe by the high energy flux (of the order of 10 MW/m^2 carried mostly by the electrons) makes it impossible to measure electron temperature below $2T_p$. Consequently, only the ion saturation current can be measured. Effectively the preceding means that the electron current is measured in the interval $(2T_p, \infty)$. Because the number of electrons absorbed by the Langmuir probe rapidly decreases as the amplitude of the positive biasing of the probe increases, the slope of the probe Volt–Ampere characteristic measured within a narrow interval ($2\text{–}4T_p$ in the case of C-Mod) around the floating potential value is

* Corresponding author. Tel.: +1-617 253 5799; fax: +1-617 253 0448; e-mail: oleg@rex.pfc.mit.edu.

PII S0022-3115(96)00532-6

interpreted as the actual temperature of the electron distribution. However, the effective temperature $T_{\rm eff}$ of the electron distribution function $f_{\rm e}(\varepsilon)$ as evaluated from

$$T_{\rm eff}(\varepsilon) = -\left(\frac{{\rm d}\ln f_{\rm e}(\varepsilon)}{{\rm d}\varepsilon}\right)^{-1}, \tag{1}$$

which is equal to $T_{\rm p}$ for a Maxwellian distribution, can be significantly larger or smaller for a non-thermal tail. As a result, probe measurements can mis-estimate the actual electron temperature.

Due to non-local effects the parallel electron distribution function is usually asymmetric, with different up- and downstream wings. If a fast-scanning (FS) probe is shielded so that it collects only electrons from either the up- or downstream sides, it can measure different temperatures $T_{\rm eff}$ at the same spatial position! As a result, kinetic effects are required to explain the experimentally measured variation of the upstream (against the flow) and downstream (towards the plate) temperatures by the reciprocating probes in Alcator C-Mod [11].

Another phenomenon for which kinetic effects are of potential importance is ELM bursts [12] in the SOL as discussed in Section 4. Experimentally observed ELM activity is characterized by a frequency of 1–10 kHz and a 10–20 times increase in the heat loading of the divertor plate. Because of the transient nature of these events, we expect that the distribution function will be incompletely equilibrated.

2. Model 1D geometry, equations and numerical method

The Fokker–Planck code ALLA solves the following kinetic equation for electron distribution function $f_{\rm e}(t, x, v, \mu)$:

$$\frac{\partial f_{\rm e}}{\partial t} + v\mu\frac{\partial f_{\rm e}}{\partial x} + \frac{1}{v^2}\frac{\partial}{\partial v}\left(v^2\mu\frac{eE_x}{m_{\rm e}}f_{\rm e}\right) + \frac{1}{v}\frac{\partial}{\partial \mu}\left[\left(1-\mu^2\right)\frac{eE_x}{m_{\rm e}}f_{\rm e}\right] = C_{\rm e}^{\rm C}. \tag{2}$$

Here $x \in (0, L)$ and is parallel to magnetic line direction, $v = \sqrt{v_{\|}^2 + v_{\perp}^2}$ = modules of velocity, $\mu \equiv v_{\|}/v$ = cosine of angle between particle velocity and x axis, e and $m_{\rm e}$ are the charge and mass of electrons, and E_x = the parallel electric field, which is obtained from Braginskii parallel momentum balance equation

$$eE_x = -0.71\frac{\partial T_{\rm p}}{\partial x} - \frac{1}{n_{\rm p}}\frac{\partial n_{\rm p}T_{\rm p}}{\partial x}. \tag{3}$$

The sheath potential is evaluated using a logical sheath boundary condition since we do not resolve sheath structure. In Eq. (2), $C_{\rm e}^{\rm C}$ is the Landau collision term, which for the Maxwellian Rosenbluth potentials $\phi_{\rm M}$ and $\psi_{\rm M}$ [13], can be expressed as

$$C_{\rm e}^{\rm C} = \frac{1}{v^2}\frac{\partial}{\partial v}v^2\sum_{\beta={\rm e,i}}\left(\frac{m_{\rm e}}{m_\beta}\frac{\partial\phi_{\rm M}^\beta}{\partial v}f_{\rm e} + \frac{\partial^2\psi_{\rm M}^\beta}{\partial v^2}\frac{\partial f_{\rm e}}{\partial v}\right) - \frac{\partial}{\partial\mu}\times\frac{1-\mu^2}{v^2}\sum_{\beta={\rm e,i}}\left(\frac{1}{v}\frac{\partial\psi_{\rm M}^\beta}{\partial v}\frac{\partial f_{\rm e}}{\partial\mu}\right). \tag{4}$$

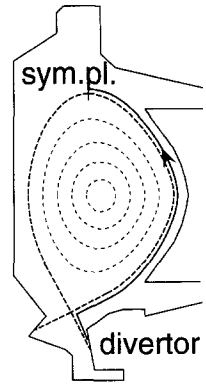

Fig. 1. Alcator C-Mod cross-section indicating simulation domain.

An Alcator C-Mod poloidal cross-section is shown in Fig. 1. The simulation domain is marked by a solid line (with an arrow) and corresponds to half of the connection length along the magnetic field line. In the adopted ID geometry, the plate is located at $x = 0$ and the symmetry plane at $x = L$. The X-point is ≈ 1 m from the plate.

Unlike Refs. [5,7–10] where a Monte-Carlo approach (which suffers from statistical fluctuations that make energetic tail resolution difficult) our numerical method uses a finite-volume approach, similar to one used in Ref. [6]. An additional improvements includes time-splitting using a cubic spline technique [14] for the free-streaming term evaluated on the adaptive non-uniform in real space grid, combined with an implicit scheme for the Coulomb operator on the non-uniform velocity space grid [15]. A typical grid size is $100(x)\times 129(v)\times 33(\mu)$. Spatial resolution near the plate (midplane) is 1 mm (10 cm). The velocity mesh varies from $0.01v_t^{\rm d}$ to $4v_t^{\rm m}$, where the indexes d and m denote divertor and midplane electron thermal velocity $v_t \equiv \sqrt{2T_{\rm p}/m_{\rm e}}$.

3. Probe measurement interpretation

To interpret probe measurements we employ the 1D-2V Fokker–Planck code ALLA [1] to study the equilibration of the electron distribution function $f_{\rm e}$ for the experimentally measured $n_{\rm p}$ and $T_{\rm p}$ profiles (from shot #950308013 at 777 ms). Plasma parameters are obtained from a conduction model reconstruction of the experimental data which

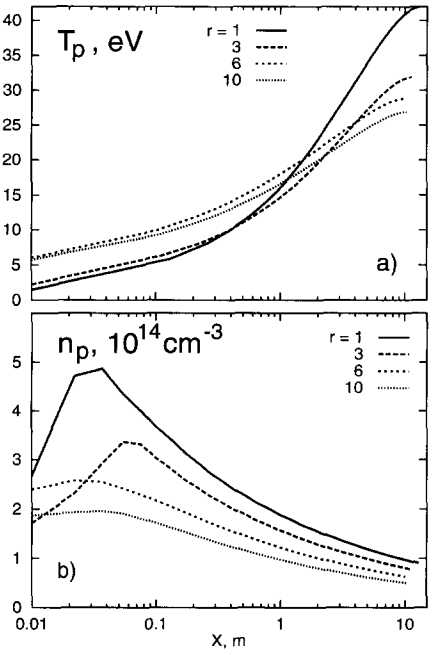

Fig. 2. (a) Background plasma temperature, T_p, and (b) density, n_p.

assumes the plasma pressure (measured by reciprocating probes) is constant along the magnetic line until the temperature drops below $T_i \approx 7$ eV. Below T_i the plasma density is obtained from the assumption that the pressure drops linearly to the plate pressure as measured by the divertor probes. The resulting plasma temperature and density are shown in Fig. 2a, b, respectively, where r denotes the distance from separatrix at the midplane for a given magnetic flux surface.

The electron distribution is evolved using the full e–e collisional term (as given by Eq. (4)) and a pitch-angle scattering term for e–i collisions. Reflecting boundary conditions (bc) are imposed at both the midplane (a symmetry assumption) and the target (where the sheath potential reflects most of the electrons). The reflecting bc is also employed to avoid introducing an ionization source to compensate for electrons lost to divertor.

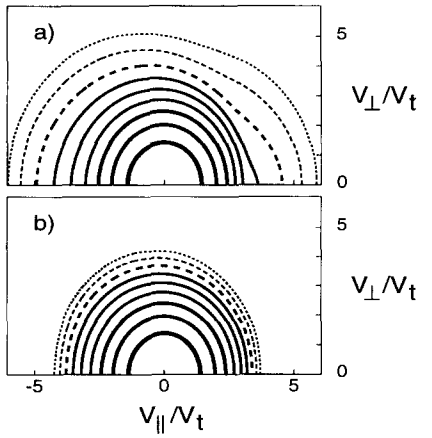

Fig. 3. Contours $f_e(v_{\|}, v_{\perp})$ at FS probes for: (a) $r = 1$ mm and (b) $r = 10$ mm.

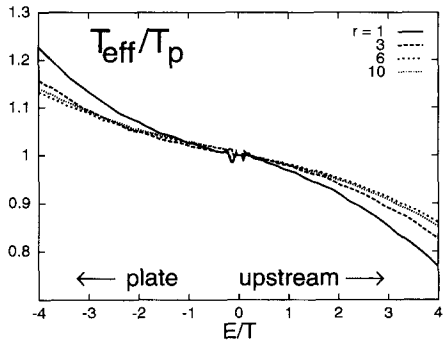

Fig. 4. Ratio T_{eff} / T_p at FS probes for different r in mm.

Contours of $\ln f_e$ for the two-dimensional distribution function evaluated at the FS probe positions for $r = 1$ mm and $r = 10$ mm are shown in Fig. 3a, b, respectively, in $v_{\|}$, $v_{\perp}$ coordinates. The plasma has about the same collisionality in both cases, however, f_e in Fig. 3b is more equilibrated than it is in Fig. 3a because of a weaker gradient in the plasma temperatures along the magnetic field line $r = 10$ mm. Another important observation from Fig. 3a, b is that due to the asymmetry of the distribution function, the parallel temperature, $T_{\|} \propto \int f_e v_{\|}^2 \, d\vec{v}$, can differ from the perpendicular temperature, $T_{\perp} \propto \int f_e v_{\perp}^2 \, d\vec{v}$. This difference can affect, for instance, the Thompson scattering measurements of electron temperature.

The ALLA code finds a Maxwellian bulk with a non-thermal tail, especially for flux surfaces near the separatrix. The ratio T_{eff}/T_p is shown in Fig. 4 for different energies. Negative (positive) values of E/T denote the downstream (upstream) wing of $f_{\|}$. The parallel distribution function is asymmetric and the variation of T_{eff} about $3T_p$ is 20–40% (depending on r), consistent with C-Mod

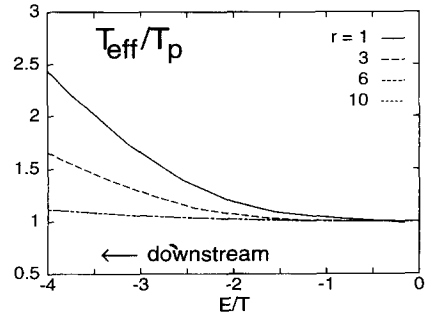

Fig. 5. Ratio T_{eff} / T_p at the divertor probes for different r in mm.

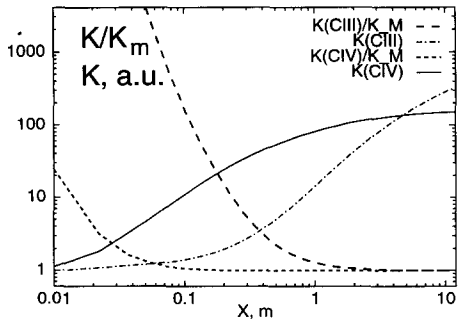

Fig. 6. Absolute values of K and ratios of K to Maxwellian value, K/K_m, for $r = 1$ mm.

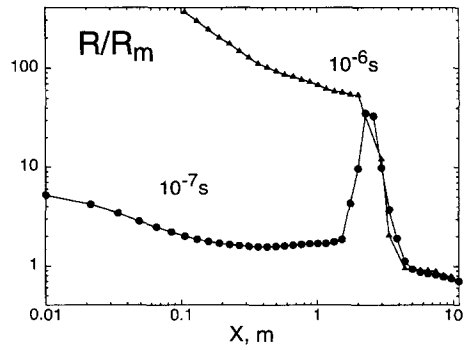

Fig. 8. Ratio R/R_M during ELM burst at two different times.

experimental observations [11]. Similar plot for the divertor probes is show in Fig. 5. The divertor probes overestimate T_p by almost a factor of two for $r \leq 1$ mm.

Next, we calculate the effective CIII and CIV excitation rates, $K = < \sigma_{CIII,IV} v >$, of carbon and the short mean-free path heat conduction coefficient [17], $R \alpha \int v^9 f d\vec{v}$, and compare them to their Maxwellian values as shown in Figs. 6 and 7.

At the midplane the electron distribution has a depleted tail, resulting in R and K being slightly below their corresponding Maxwellian quantities. However, due to non-local effects driven by very steep temperature gradients in the region near the plate, both the plasma heat conduction coefficient and impurity radiation rates are dramatically altered (up to two orders of magnitude!). Note that the absolute value of the CIII excitation constant, K, varies along the magnetic line much less than its relative value, K/K_m. To obtain the total radiation loss, K has to be multiplied by impurity density.

Finding the distribution function of the impurity charge states along the magnetic line is beyond the scope of this investigation. However, from Fig. 6 one sees that kinetic effects can have a strong impact on both impurity radiation and the impurity distribution over different charge states (by affecting impurity ionization rate constant), and should be taken into account in fluid codes [16].

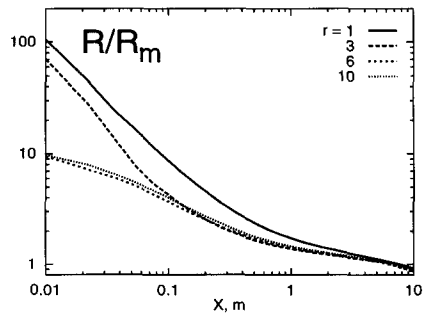

Fig. 7. Ratios of R to Maxwellian value, R/R_m, for different flux surfaces.

4. Kinetic model of ELM bursts

One-dimensional velocity space models of ELM bursts were studied in [1,18]. There the initial ELM propagation (heating) stage was modeled by increasing the background plasma temperature used to evaluate the Maxwellian Rosenbluth potentials, while the final (cooling) stage was modeled using a Krook operator which mainly affected the energetic particles. The incomplete Maxwellization of the electron distribution function was considered, and the analytical solutions found were used to benchmark our Fokker–Planck code.

In the present work we simulate a 1D-2V ELM burst using the following simplified model. We solve the same Eq. (2), but in this case we allow the temperature in the Maxwellian Rosenbluth potentials of the background plasma to vary in time. The initial profile approximately corresponds to detached flow in C-Mod for $r = 6$ mm. The temperature of the background is increased 10 times (up to 300 eV at the midplane) in the spatial interval $[1/3L, L]$ during a time of about 10^{-6} s.

The preliminary results are the following. The parallel distribution function $f_{\|}$ obtained from this model is asymmetric with the downstream wing having an enhanced energetic tail and upstream wing depleted. Due to this non-Maxwellian behavior, the heat conduction coefficient R exceeds the equilibrium one by factor of 30 in the region around the thermal as shown in Fig. 8.

5. Conclusion

The results of our kinetic modeling of a detached Alcator C-Mod SOL plasma can be summarized as follows. Non-local kinetic effects are shown to be responsible

for the asymmetry in the FS probe measurements and the higher electron temperatures measured by divertor plate Langmuir probes in C-Mod. The non-local behavior is also shown to have a large effect on electron heat conduction and impurity radiation rates. This nonlocal behavior is increasingly important for detached plasma flows and ELM bursts, which are characterized by sharp temperature gradients.

Acknowledgements

Work performed under the auspices of the United States Department of Energy by MIT under Contracts DE-FG02-91-ER-54109 and DE-AC02-78ET51013, and by Lodestar under Contract DE-FG02-88-ER-53263.

References

[1] A.A. Batishcheva et al., Phys. Plasmas 3 (1996) 1634.
[2] E.M. Epperlein, Phys. Rev. Lett. 69 (1992) 1765.
[3] I.H. Hutchinson et al., Phys. Plasmas 1 (1994) 1511.
[4] S.I. Braginskii, Rev. Plasma Phys. (Consultants Bureau, NY) 1 (1965) 205.
[5] S.A. Khan and T.D. Rognlien, Phys. Fluids 24 (1981) 1442.
[6] L.M. Montierth, R.L. Morse and W.A. Neuman, Phys. Fluids B 1 (1989) 1911–1925.
[7] S.I. Krasheninnikov et al., J. Nucl. Mater. 196–198 (1992) 899.
[8] R.H. Cohen and T.D. Rognlien, Contrib. Plasma Phys. 34 (1994) 198.
[9] O.V. Batishchev et al., Contrib. Plasma Phys. 34 (1994) 436.
[10] O.V. Batishchev et al., Phys. Plasmas 3(9) (1996).
[11] B. LaBombard, private communication.
[12] H. Zohm et al., Nucl. Fusion 32 (1992) 489.
[13] B.A. Trubnikov, Rev. Plasma Phys. (Consultants Bureau, NY) 1 (1965) 105.
[14] M.M. Shoucri and G. Gagne, J. Comput. Phys. 27 (1978) 315.
[15] A.A. Batishcheva et al., Contrib. Plasma Phys. 36(2/3) (1996) 414.
[16] F. Wising et al., Contrib. Plasma Phys. 36(2/3) (1996) 136.
[17] J.A. Albritton et al., Phys. Rev. Lett. 57 (1986) 1887.
[18] D.J. Sigmar et al., Contrib. Plasma Phys. 36(2/3) (1996) 230.